Structure and Electrochemical Performance of $LiNi_yCo_{0.1-y}Mn_{1.9}O_4$ Cathode Materials Prepared by a Precipitation Method *

WANG, Guo-Guang[1] WANG, Jian-Ming[1] MAO, Wen-Qu[1] LIU, Li-Qing[1]
ZHANG, Jian-Qing[1,2] CAO, Chu-Nan[1,2]

([1]*Department of Chemistry, Zhejiang University, Hangzhou 310027*; [2]*State Key Laboratory for Corrosion and Protection, Institute of Metal Research, Chinese Academy of Sciences, Shenyang 110016*)

Abstract Spinel $LiMn_2O_4$ and $LiNi_yCo_{0.1-y}Mn_{1.9}O_4$ (y=0, 0.05, 0.10) samples were prepared by a precipitation method. The structure, morphology, and electrochemical performance of the samples were characterized by Fourier transform infrared (FT-IR) spectroscopy, X-ray diffraction (XRD), scanning electron micrographs (SEM), charge-discharge measurements, and electrochemical impedance spectra (EIS). The results of FT-IR and XRD indicated that the absorption band at about 519 cm^{-1} shifts to the high frequency with the decrease of Ni content in $LiNi_yCo_{0.1-y}Mn_{1.9}O_4$ samples and the lattice parameter(a) of $LiMn_2O_4$ samples decreases with the addition of Ni, Co, or Ni/Co. The SEM observation displayed that the $LiNi_yCo_{0.1-y}Mn_{1.9}O_4$ samples have lower agglomeration degree and smaller particle size. The results of the electrochemical experiments showed that the improvements on the electrochemical performance of substituted samples have some different reasons, and the $LiNi_{0.05}Co_{0.05}Mn_{1.9}O_4$ sample manifests better electrochemical performance in 4 V region due to its lower electrochemical polarization and larger diffusion coefficient of Li^+ ions.

Keywords: Lithium ion batteries, Substituted manganese spinel oxide, Precipitation, Electrochemical properties

Lithium-ion batteries have become attractive power sources for portable electronic devices due to their high energy density. Commercial lithium-ion batteries currently utilize the layered $LiCoO_2$ cathode, because it has large specific capacity, high operating voltage and excellent rechargeability. The spinel $LiMn_2O_4$ is appealing for its low cost, high environmental acceptability and relatively large energy densities, compared with $LiCoO_2$, $LiNiO_2$ and $LiNi_zCo_{1-z}O_2$[1-6]. However, $LiMn_2O_4$ suffers from both the inferior theoretical capacity (148 $mAh\cdot g^{-1}$, compared with 274 $mAh\cdot g^{-1}$ of $LiCoO_2$) and a fast performance fade. This capacity fading has been attributed to spinel dissolution[7], the Jahn-Teller effect[8], and lattice instability[9]. There has been much work[10-21] in recent years to stabilize $LiMn_2O_4$ cathodes with various metal elements such as Al, Mg, Co, Ni, Fe, Ti, Zn, Cr and Cu. The substituted $LiMn_2O_4$ showed improved cycle life at the expense of capacity.

It is well known that the physicochemical properties of any material have close relation with its synthesis method. In general, $LiM_xMn_{2-x}O_4$(M=Co, Ni, Cr, etc.) material was prepared by a conventional solid-state method at low(600~700 ℃) or high (750~850 ℃)[22-23] temperatures. In this process, the oxides or carbonates containing manganese and lithium cations are physically mixed by mechanical methods, and the solid particles may not completely react, which results in undesirable impurities in the final product. Therefore, considerable improvements on the preparation of $LiM_xMn_{2-x}O_4$ cathode materials have been accomplished by the wet method[24-26]. All the components can be homogeneously distributed in the samples prepared by these wet methods. Single phase products with good crystallizability, homogeneity and uniform particle morphology were obtained, which exhibited high electrochemical activity. But the soft chemistry methods for prepare cathode materials are complicated and restricted, so it is valuable to explore simple and controllable methods of preparing $LiMn_2O_4$ samples with high activity

Received: April 5, 2005; Revised: May 9, 2005. Correspondent: WANG, Jian-Ming (E-mail: wjm@cmsce.zju.edu.cn; Tel: 0571-87951513; Fax: 0571-87953309). *The Project Supported by NSFC (59902004)

and homogeneous particle morphology.

Huang *et al*.[27] prepared the precursor of $LiMn_2O_4$ sample from $Mn(CH_3COO)_2\cdot 4H_2O$ and Li_2CO_3 by a simple liquid-state precipitation method. The final $LiMn_2O_4$ sample with initial discharge capacity of 110 $mAh\cdot g^{-1}$ and relatively good capacity retention was obtained by calcining the precursor at 600 ℃. However, the properties of the substituted $LiMn_2O_4$ samples prepared by the above method have not been investigated.

In our previous work[28], the method of synthesizing $LiMn_2O_4$ has been improved on the basis of the Ref.[27]. In this paper, $LiNi_yCo_{0.1-y}Mn_{1.9}O_4$ (y=0, 0.05, 0.1) samples were synthesized by the improved method, and the effects of the addition of Co and Ni on the structure and electrochemical performance of $LiMn_2O_4$ samples are studied in detail.

1 Experimental

1.1 Preparation of $LiMn_2O_4$ and $LiNi_yCo_{0.1-y}Mn_{1.9}O_4$ (y=0, 0.05, 0.1) samples

In order to obtain $LiNi_yCo_{0.1-y}Mn_{1.9}O_4$ samples, Li_2CO_3, $Ni(CH_3COO)_2\cdot 4H_2O$, $Co(CH_3COO)_2\cdot 4H_2O$ and $Mn(CH_3COO)_2\cdot 4H_2O$ with 1:y:(0.1−y):1.9 mole ratio of Li∶Ni∶Co∶Mn were dissolved in distilled water. A precipitate (the precursor) was obtained by evaporating water with continual stirring at 95 ℃. The precursor was transferred into a ceramic crucible, subsequently calcined in a Nabertherm furnace at 800 ℃ for 8 h and then cooled slowly to room temperature in air. The $LiMn_2O_4$ sample was obtained from Li_2CO_3 and $Mn(CH_3COO)_2\cdot 4H_2O$ with 1:2 mole ratio of Li∶Mn by the same method.

1.2 Physical characterization of samples

The Fourier transform infrared (FT-IR) spectroscopy of the samples was performed using a Nicolet Nexus 360 FT-IR spectrophotometer. The frequency range was 1500～250 cm^{-1}. The crystal structure of the samples was determined by X-ray diffraction (XRD) analysis using X-ray diffractometer (Rigaku D/Max 2550) with Cu K_α radiation at 40 kV and 300 mA, and a scanning rate (2θ) of 8 (°)·min^{-1}. The morphologies of the samples were examined using scanning electron microscopy (SEM) (Sirion, Edax).

1.3 Preparation of electrodes and electrochemical tests

The charge and discharge characteristics of $LiMn_2O_4$ and $LiNi_yCo_{0.1-y}Mn_{1.9}O_4$ cathode were examined in two-electrode test cells. The cells consisted of a cathode and a lithium metal anode separated by a microporous polypropylene separator. The electrolyte used was 1 $mol\cdot L^{-1}$ $LiPF_6$ in a 50/50 (V/V) mixture of ethylene carbonate(EC) / dimethyl-carbonate(DMC). The cathode consisted of a mixture of 80%(w) sample, 10% (w) acetylene black and 10%(w) polyvinylidene fluoride (PVDF). The mixture was pressed onto an aluminum foil at 250 $kg\cdot cm^{-2}$ and vacuum-dried at 120 ℃ for 12 h. The cathode was cycled in the potential range of 3.0～4.3 V *vs* Li/Li^+ electrode at room temperature at 0.5 C rate. Electrochemical impedance spectroscopy (EIS) measurements were performed using a Swagelock three-electrode cell[29] by Potentiosta/Galvanostat Model 273A in conjunction with a model 5210 lock-in amplifier. A typical cathode was prepared by mixing 80%(w) sample, 10%(w) acetylene black, and 10%(w) PVDF and roll-pressed into a thin disk approximately 110 μm in thickness and 2.40 cm in diameter. The counter electrode and reference electrode were made of Li foil. In EIS measurement the range of frequency was between 0.005 Hz and 120 kHz and the excitation amplitude was 5 mV. All assembling of the cell was carried out in a glove box filled with Ar gas.

2 Results and discussion

2.1 Physical properties of samples

In order to investigate the effects of different additives on spinel $LiMn_2O_4$ structure, the infrared spectra within the frequency range 1500～250 cm^{-1} of $LiMn_2O_4$ and $LiNi_yCo_{0.1-y}Mn_{1.9}O_4$ samples were shown in Fig.1. Two main absorption bands occur at 613 and 519 cm^{-1}, which are attributed to the asymmetric stretching modes of MnO_6 group. It is clear that the frequency of absorption band at about 519 cm^{-1} of $LiNi_yCo_{0.1-y}Mn_{1.9}O_4$ samples is lower than that of $LiMn_2O_4$ sample, and the absorption band at 519 cm^{-1} shifts to the high frequency with the decrease of Ni content in $LiNi_yCo_{0.1-y}Mn_{1.9}O_4$ samples, namely, the increase of Co content. This might be related to the atomic mass and the

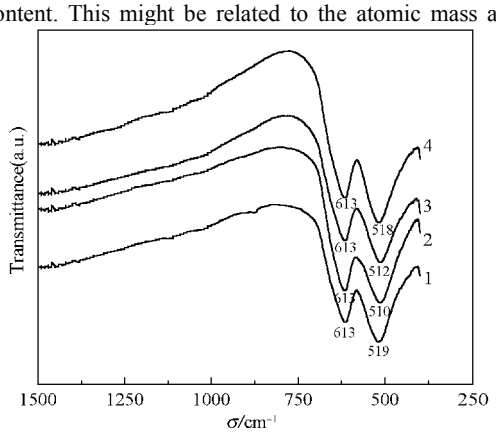

Fig.1 FT-IR spectra of different samples

1) $LiMn_2O_4$, 2) $LiNi_{0.1}Mn_{1.9}O_4$, 3)$LiNi_{0.05}Co_{0.05}Mn_{1.9}O_4$, 4) $LiCo_{0.1}Mn_{1.9}O_4$

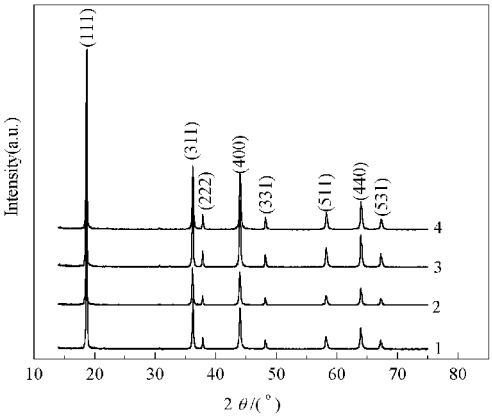

Fig.2 XRD patterns of different samples

1) $LiMn_2O_4$, 2) $LiNi_{0.1}Mn_{1.9}O_4$, 3) $LiNi_{0.05}Co_{0.05}Mn_{1.9}O_4$, 4) $LiCo_{0.1}Mn_{1.9}O_4$

ionic radius of transition metal and the bonding energy of the M—O (M=Mn, Ni, Co). The effect of atomic mass of an additive substituted for Mn on the characteristic frequency of Mn(III)—O is consistent with that of its ionic radius, but contrary to that of the bonding energy of the M—O. The additive with larger atomic mass and ionic radius than Mn can lead to the decrease in the frequency of Mn(III)—O[30]. Since Ni^{2+} or Co^{3+} ions have similar even smaller ionic radii compared with manganese ions, the atomic mass of Ni or Co is larger than that of Mn, and the bonding energy of the M—O (M=Ni, Co) is larger than that of Mn—O (the binding energies of Mn—O, Ni—O and Co—O are 946, 1029 and 1142 $kJ\cdot mol^{-1}$ [31], respectively), the degree of shift is different for the frequency of Mn(III)—O.

The XRD patterns of the samples are shown in Fig.2. The unit cell data of the samples are listed in Table 1. The diffraction patterns of all samples show the characteristics of spinel $LiMn_2O_4$ structure(JCPDS 35-782) with a space group *Fd*3*m* in which the lithium ions occupy the tetrahedral(8a) sites and the transition metal ions reside at the octahedral (16d) sites, indicating that basic $LiMn_2O_4$ structure is not changed by partial substitution of Ni, Co, and Ni/Co for manganese in the sample. It can be seen from Table 1 that the $LiMn_2O_4$ and $LiNi_yCo_{0.1-y}Mn_{1.9}O_4$ samples can be ranked in term of the lattice parameter (*a*) as follows:$LiMn_2O_4 > LiNi_{0.1}Mn_{1.9}O_4 > LiNi_{0.05}Co_{0.05}Mn_{1.9}O_4 > LiCo_{0.1}Mn_{1.9}O_4$. This is because not only the doped ions have similar even smaller ionic radius, compared with manganese ions, i.e., Ni^{2+} (0.068 nm), Mn^{3+}(0.065 nm), Co^{3+}(0.0545 nm) [32], but also the bonding energy of the M—O(M=Ni, Co) is larger than that of the Mn—O bond. The decrease in cell volume and the stronger M—O (M=Ni, Co) bond should increase the stability of the structure during intercalation and deintercalation of Li^+ ions.

Table 1 The cell parameters and cell volumes of the samples

Sample	Lattice parameter(*a*/nm)	Unit cell volume(nm^3)
$LiMn_2O_4$	0.82337	0.55821
$LiNi_{0.1}Mn_{1.9}O_4$	0.82332	0.55809
$LiNi_{0.05}Co_{0.05}Mn_{1.9}O_4$	0.82260	0.55663
$LiCo_{0.1}Mn_{1.9}O_4$	0.82253	0.55648

Fig.3 displays the scanning electron micrographs (SEM) of $LiMn_2O_4$ and $LiNi_yCo_{0.1-y}Mn_{1.9}O_4$ samples. The $LiMn_2O_4$ sample appears as aggregates of irregular shape, and its particle size is much larger than those of other samples. The additions of Ni, Co, and Ni/Co decrease the agglomeration degree of the samples and their particles become smaller and more uniform. It is also noted that the sample with Ni/Co manifests relatively larger particle size and better crystallinity than the samples with Ni or Co.

2.2 Electrochemical performance of samples

Fig.4 illustrates the first charge-discharge curves of $LiMn_2O_4$ and $LiNi_yCo_{0.1-y}Mn_{1.9}O_4$ samples at 0.5*C* in the voltage range of 3.0 ~ 4.3 V. It can be seen that both the charge curves and the discharge ones display two distinct potential plateaus, which correspond to different transition equilibrium between various oxide states of Mn[33], respectively. The upper plateau region of discharge curve represents a two-phase equilibrium between λ-MnO_2 and $Li_{0.5}Mn_2O_4$, while the second plateau represents another phase equilibrium between $Li_{0.5}Mn_2O_4$ and $LiMn_2O_4$. The $LiNi_yCo_{0.1-y}Mn_{1.9}O_4$ samples display higher discharge potential and larger discharge capacity than the $LiMn_2O_4$ sample. The compositions of $LiNi_{0.1}Mn_{1.9}O_4$ and $LiCo_{0.1}Mn_{1.9}O_4$ can be rewritten as $LiNi^{2+}_yMn^{3+}_{1-2y}Mn^{4+}_{1+y}O^{2-}_4$ and $LiCo^{3+}_yMn^{3+}_{1-y}Mn^{4+}O^{2-}_4$ (y=0. 1)[34-35]. Since the deintercalation of Li^+ from the spinel structure must be electrically compensated by the oxidation of Mn^{3+} to Mn^{4+}, the initial capacities of $LiMn_2O_4$ and $LiNi_yCo_{0.1-y}Mn_{1.9}O_4$ are limited by the initial amount of Mn^{3+} in the 16d sites. Thus, in this case, an amount equivalent to $(1-2y)$ of Li in $LiNi_{0.1}Mn_{1.9}O_4$ sample and $(1-y)$ of Li in $LiCo_{0.1}Mn_{1.9}O_4$ can be intercalated-deintercalated

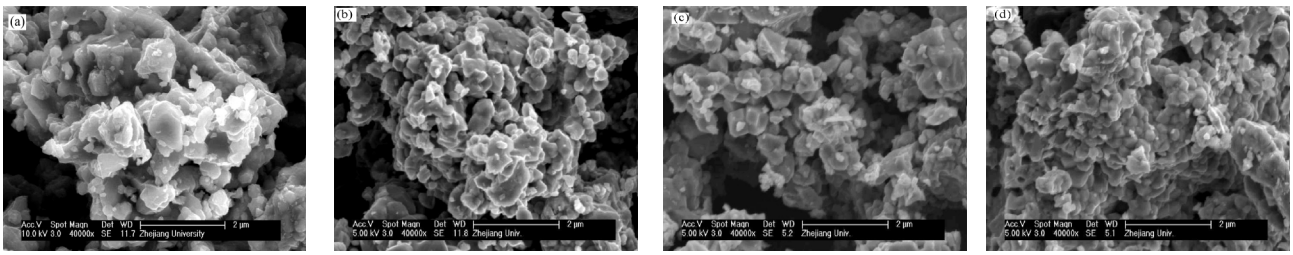

Fig.3 SEM photos of different samples

(a) $LiMn_2O_4$, (b) $LiNi_{0.1}Mn_{1.9}O_4$, (c) $LiNi_{0.05}Co_{0.05}Mn_{1.9}O_4$, (d) $LiCo_{0.1}Mn_{1.9}O_4$

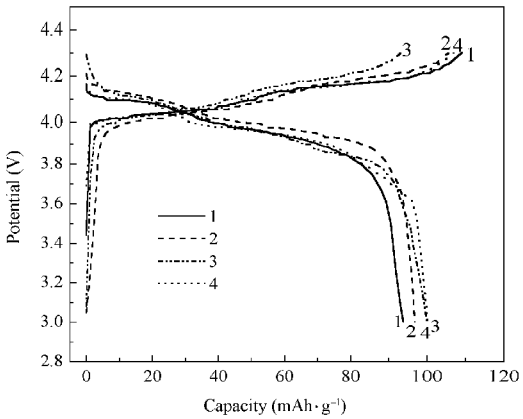

Fig.4 The first charge-discharge curves of different samples at 0.5*C* rate

1) $LiMn_2O_4$, 2) $LiNi_{0.1}Mn_{1.9}O_4$, 3) $LiNi_{0.05}Co_{0.05}Mn_{1.9}O_4$, 4) $LiCo_{0.1}Mn_{1.9}O_4$

during cycling over the voltage range. On this basis, the calculated capacities of $LiNi_{0.1}Mn_{1.9}O_4$, $LiNi_{0.05}Co_{0.05}Mn_{1.9}O_4$, and $LiCo_{0.1}Mn_{1.9}O_4$ samples are 118, 125 and 133 mAh·g^{-1}, respectively. The differences between the calculated and experimental capacities indicate that only 0.80～0.85 mol Li^+ per mol of the lithium manganese oxide can be intercalated-deintercalated within the voltage range of cycling. It should be noted that the discharge capacity of $LiMn_2O_4$ is lower than that of $LiNi_yCo_{0.1-y}Mn_{1.9}O_4$ in our experiments, which is some different from other research work [34-35]. This difference may be caused by various characteristics of the $LiMn_2O_4$ sample. The particle aggregation of the $LiMn_2O_4$ sample in our work hinders electrolyte from penetrating through the particles, which is disadvantageous to the intercalation and deintercalation of Li^+ and results in the decrease of discharge capacity.

The cycle behavior of $LiMn_2O_4$ and $LiNi_yCo_{0.1-y}Mn_{1.9}O_4$ samples at 0.5*C* rate between 3.0 and 4.3 V is presented in Fig.5. The discharge capacity retention ratios are calculated by dividing the delivered capacity at a given cycle with the first cycle capacity except that the ratio for $LiCo_{0.1}Mn_{1.9}O_4$ is calculated by dividing the delivered capacity with the second cycle capacity. It can be seen that the discharge capacities of $LiNi_yCo_{0.1-y}Mn_{1.9}O_4$ samples increase with the decrease of y value in the samples from y=0.1 to y=0, but all are larger than that of the $LiMn_2O_4$ sample. For $LiMn_2O_4$, $LiNi_{01}Mn_{19}O_4$, $LiNi_{005}Co_{005}Mn_{19}O_4$ and $LiCo_{01}Mn_{19}O_4$ samples the discharge capacity retention ratios after 30 cycles is 85%, 90%, 95% and 93%, respectively. Owing to the distortion of the unit cell during cycling, the capacity of pure $LiMn_2O_4$ has a relatively large deterioration rate during electrochemical cycling. The $LiNi_yCo_{0.1-y}Mn_{1.9}O_4$ samples display better cyclic performance than pure $LiMn_2O_4$. This is ascribed to the fact that the unit-cell volume decreases with the decrease of y value in the $LiNi_yCo_{0.1-y}Mn_{1.9}O_4$ samples and the bonding energy of the M—O (M=Ni, Co) is larger than that of the Mn—O bond (Co—O > Ni—O > Mn—O), which improves the stability of the spinel structure and lowers the capacity loss of the $LiNi_yCo_{0.1-y}Mn_{1.9}O_4$($y$=0, 0.05, 0.10) samples during electrochemical cycles. In addition, the relatively better crystallinity of $LiNi_yCo_{0.1-y}Mn_{1.9}O_4$ samples may have some contributions to their better electrochemical cycle stability. The relatively larger particle size and improved crystallinity might be the reason why the $LiNi_{0.05}Co_{0.05}Mn_{1.9}O_4$ sample has the largest capacity retention after 30 cycles.

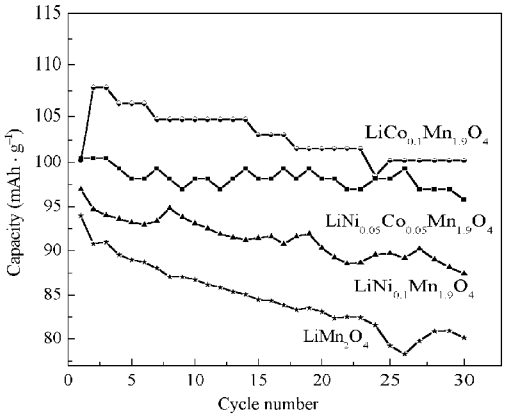

Fig.5 The cycle performance of different samples at 0.5*C* rate

In order to further investigate the effects of substitution on the kinetic process of the electrodes, the electrochemical impedance spectra (EIS) of the electrodes prepared from the $LiMn_2O_4$ and $LiNi_yCo_{0.1-y}Mn_{1.9}O_4$ samples were measured (Fig.6). It is well known that the impedance spectroscopy of manganese spinels depends on the potential[36-37]. Here, all the measurements were done at 4.10 V during the discharge. The Nyquist plots obtained show the curves similar with those previously reported for manganese-containing spinels. A small high-frequency semicircle results from

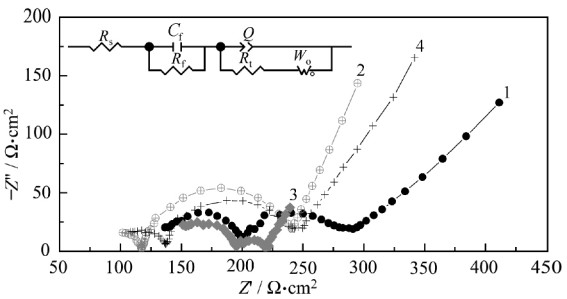

Fig.6 Typical Nyquist plots of different samples at 4.10 V during the discharge and their equivalent circuit

1) $LiMn_2O_4$, 2) $LiNi_{0.1}Mn_{1.9}O_4$, 3) $LiNi_{0.05}Co_{0.05}Mn_{1.9}O_4$, 4) $LiCo_{0.1}Mn_{1.9}O_4$

Table 2 Some parameters obtained by EIS fitting

Samples	R_s /Ω·cm²	R_f /Ω·cm²	R_t/Ω·cm²	W_o/Ω·cm²
$LiMn_2O_4$	135.49	62.73	97.60	98.19
$LiNi_{0.1}Mn_{1.9}O_4$	87.39	30.10	123.75	69.12
$LiCo_{0.1}Mn_{1.9}O_4$	102.46	33.30	100.39	41.53
$LiNi_{0.05}Co_{0.05}Mn_{1.9}O_4$	143.82	46.30	30.64	31.86

the resistance (R_f) for Li^+ ions migration through the surface films and film capacitance(C_f)[38-40]. The middle-frequency capacitive loop is caused by the charge transfer resistance (R_t) and interfacial capacitance (C_{dl}), and the low-frequency straight line originates from the diffusion of Li^+ ions in the solid cathode matrix. The fitted results of EIS using the equivalent circuit shown in Fig.6 are displayed in Table 2. This circuit is very similar with those previously reported in the literature[41-43]. According to a usual assignment, R_s is the ohmic resistance, R_f and C_f are the resistance and capacitance of a solid electrolyte interphase (SEI) film, respectively. W_o is the Warburg impedance of the solid phase diffusion, and Q is a constant phase element.

At 4.10 V during the discharge, the electrochemical process is controlled by both the kinetics of charge transfer and the diffusion factors. From the fitting results of EIS, it can be seen that the $LiNi_{0.1}Mn_{1.9}O_4$ and $LiCo_{0.1}Mn_{1.9}O_4$ samples have smaller R_s values than the $LiMn_2O_4$ sample, which indicates that the addition of Ni or Co decreases the ohmic resistance of the electrodes, but the addition of Ni/Co does not change the R_s value. The smaller R_f values of $LiNi_yCo_{0.1-y}Mn_{1.9}O_4$ samples indicate that the presence of the dopants inhibits the passivation processes occurring on the surface of the cathode, decreases the resistance of SEI film and facilitates the Li^+ diffusion *via* the SEI film. It can also be seen from Table 2 that the addition of Ni or Co does not change the R_t value, but it greatly decreases the W_o value. Especially for $LiNi_{0.05}Co_{0.05}Mn_{1.9}O_4$ sample, the addition of Ni/Co sharply decreases the R_t and W_o values, which implies that the electrode has much lower electrochemical and diffusion polarizations. This may be the reason why the $LiNi_{0.05}Co_{0.05}Mn_{1.9}O_4$ sample shows higher discharge potential, larger initial discharge capacity and better cycle performance.

3 Conclusions

(1) $LiNi_yCo_{0.1-y}Mn_{1.9}O_4$($y$=0, 0.05, 0.10) cathode material has been prepared by an improved precipitation method which offers better homogeneity, preferred surface morphology, reduced heat-treatment conditions, and better crystallinity. Because of the difference in the bonding energy of the M—O (M=Mn, Ni, Co) and ionic radii of Mn^{3+}, Ni^{2+} and Co^{3+}, the lattice parameter (a) of lithium manganese oxide can be ranked as follows: $LiMn_2O_4$ > $LiNi_{0.1}Mn_{1.9}O_4$ > $LiNi_{0.05}Co_{0.05}Mn_{1.9}O_4$ > $LiCo_{0.1}Mn_{1.9}O_4$.

(2) The initial specific capacities of $LiMn_2O_4$, $LiNi_{0.1}Mn_{1.9}O_4$ and $LiCo_{0.1}Mn_{1.9}O_4$ samples at 0.5C rate are 94, 97, 101 and 101 mAh·g^{-1}, respectively. The substituted samples display better cycle performance than the pure $LiMn_2O_4$ sample, and the $LiNi_{0.05}Co_{0.05}Mn_{1.9}O_4$ sample has larger capacity retention ratio than the single-doped samples.

(3) The additions of Ni, Co and Ni/Co decrease the ohmic polarization of the electrodes, and improve the diffusion of Li^+. Moreover, the addition of Ni/Co obviously decreases the electrochemical polarization of the electrode.

References

1 Koksbang, R.; Barker, J.; Shi, H.; Saïdi, M. Y. *Solid State Ionics,* **1996, 84**: 1

2 Scrosati, B. *Electrochim. Acta,* **2002, 45**: 2461

3 Amine, K.; Tukamoto, H.; Yasuka, H.; Fujila, Y. *J. Electrochem. Soc.,* **1996, 143**: 1607

4 Ozawa, K. *Solid State Ionics,* **1994, 69**: 212

5 Ebner, W.; Fouchard, D.; Xie, L. *Solid State Ionics,* **1994, 69**: 238

6 Gumow, R. J.; Thackeray, M. M. *J. Electrochem. Soc.,* **1993, 140**: 3365

7 Jang, D. H.; Shin, J. Y.; Oh, S. M. *J. Electrochem. Soc.,* **1996, 143**: 2004

8 Gumow, R. J.; Kock, A.; Thackeray, M. M. *Solid State Ionics,* **1994, 69**: 59

9 Yamada, A. *J. Solid State Chem.,* **1996, 122**: 160

10 Song, D.; Ikuta, H.; Unchida, T.; Wakihara, M. *Solid State Ionics,* **1999, 117**: 151

11 Julien, C.; Ziolkiewicz, S.; Lemal, M.; Massot, M. *J. Mater. Chem.,* **2001, 11**: 1837

12 Jeong, I. S.; Kim, J. U.; Gu, H. B. *J. Power Sources,* **2001, 102**: 55

13 Kumar, G.; Schlorb, H.; Rahner, D. *Mater. Chem. Phys.,* **2001, 70**: 117

14 Bang, H. J.; Donepudi, V. S.; Prakash, J. *Electrochim. Acta,* **2002, 48**: 443

15 Banov, B.; Todorov, Y.; Trifonova, A.; Momchilov, A.; Manev, V. *J. Power Sources,* **1997, 68**: 578

16 Amine, K.; Tukamoto, H.; Yasuda, H.; Fujita, Y. *J. Power Sources,* **1997, 68**: 604

17 Feng, Q.; Hanoh, H.; Miyai, Y.; Ooi, K. *Chem. Mater.,* **1995, 7**: 379

18 Appetecchi, G. B.; Scrosati, B. *J. Electrochem. Soc.,* **1997, 144**: L138

19 Myung, S. T.; Komaba, S.; Hirosaki, N.; Kumagai, N. *Electrochem. Commun.,* **2002, 4**: 397

20 Zhang, D.; Popov, B. N.; White, R. E. *J. Power Sources,* **1998, 76**: 81

21 Ein-Eli, Y.; Lu, S. H.; Rzeznik, M. A. G. B.; Mukerjee, S.; Yang, X. Q.; McBreen, J. *J. Electrochem. Soc.,* **1998, 145**: 3383

22 Ein-Eli, Y.; Howard, W. F. *J. Electrochem. Soc.,* **1997, 144**: L205

23 Kawai, H.; Nagata, M.; Tukamoto, H.; West, A. R. *Electrochem. Solid-State Lett.,* **1998, 1** (5): 212

24 Lee, Y. S.; Sun, Y. K.; Nahm, K. S. *Solid State Ionics,* **1998, 109**: 285

25 Sun, Y. K.; Jeon, Y. S.; Lee, H. J. *Electrochem. Solid-State Lett.,* **2000, 3**(1): 7

26 Lee, Y. S.; Sun, Y. K.; Ota, S.; Miyashita, T.; Yoshio, M. *Electrochem. Commun.,* **2002, 4**: 989

27 Huang, H. T.; Bruce, P. G. *J. Electrochem. Soc.,* **1994, 141**: L106

28 Wang, G. G.; Wang, J. M.; Mao, W. Q.; Shao, H. B.; Zhang, J. Q.; Cao, C. N. *J. Solid State Electrochem.,* (Published on line: Nov. 16, 2004)

29 Yu, P.; Popov, B. N.; Ritter, J. A.; White, R. E. *J. Electrochem. Soc.,* **1999, 146**: 8

30 Feng, C. Q.; Zhang, K. L.; Sun, J. T. *J. Functional Materials (Supplement),* **2001, 32**: 1144 [冯传奇, 张克立, 孙聚堂. 功能材料(*Gongneng Cailiao*) (增刊), **2001, 32**: 1144]

31 Li, G. H.; Ikuta, H.; Uchida, T.; Wakihara, M. *J. Electrochem. Soc.,* **1996, 143**: 178

32 Liu, R. S.; Shen, C. H. *Solid State Ionics,* **2003, 157**: 95

33 Ohzuku, T.; Kitagawa, M.; Hirai, T. *J. Electrochem. Soc.,* **1990, 137**: 769

34 Zhong, Q. M.; Bonakdarpour, A.; Zhang, M. J.; Gao, Y.; Dahn, J. R. *J. Electrochem. Soc.,* **1997, 144**: 205

35 Amine, K.; Tukamoto, H.; Yasuda, H.; Fujita, Y. *J. Electrochem. Soc.,* **1996, 143**: 1607

36 Wu, X.; Kim, S. B. *J. Power Sources,* **2002, 109**: 53

37 Alcántara, R.; Jaraba, M.; Lavela, P.; Tirado, J. L. *J. Electroanal. Chem.,* **2004, 566**: 187

38 Levi, M. D.; Aurbach, D. *J. Phys. Chem. B,* **1997, 101**: 4630

39 Levi, M. D.; Levi, E. A.; Aurbach, D. *J. Electroanal. Chem.,* **1997, 421**: 89

40 Aurbach, D.; Levi, M. D.; Levi, E. A. *J. Electrochem. Soc.,* **1998, 145**: 3024

41 Levi, M. D.; Aurbach, D. *J. Phys. Chem. B,* **2004, 108**: 11693

42 Levi, M. D.; Salitra, G.; Markovsky, B.; Teller, H.; Aurbach, D. *J. Electrochem. Soc.,* **1999, 146**: 1279

43 Levi, M. D.; Gamolsky, K.; Heider, U.; Oesten, R.; Aurbach, D. *Electrochim. Acta,* **2000, 45**: 1781

$LiNi_yCo_{0.1-y}Mn_{1.9}O_4$ 正极材料的沉淀法制备及其结构与电化学性能*

王国光[1] 王建明[1] 毛文曲[1] 刘立清[1] 张鉴清[1,2] 曹楚南[1,2]

([1] 浙江大学化学系, 杭州 310027; [2] 中国科学院金属研究所, 金属腐蚀与防护国家重点实验室, 沈阳 110016)

摘要 采用沉淀法制备了尖晶石型 $LiMn_2O_4$ 和 $LiNi_yCo_{0.1-y}Mn_{1.9}O_4$ (y=0, 0.05, 0.1)正极材料. 应用 FT-IR、XRD 和 SEM 技术对不同掺杂样品的相结构与形貌进行了表征, 并用恒电流充放电测试和电化学阻抗技术研究了样品的电化学行为. FT-IR、XRD 和 SEM 结果显示: 随着掺杂型 $LiNi_yCo_{0.1-y}Mn_{1.9}O_4$ 样品中 Ni 含量的减少, 位于 519 cm^{-1} 处的红外峰向高频方向移动; Ni、Co 或 Ni/Co 的掺杂降低了 $LiMn_2O_4$ 的晶格参数; 掺杂型 $LiNi_yCo_{0.1-y}Mn_{1.9}O_4$ 样品具有更好的分散度和小的粒径. 电化学实验结果表明, 不同成分的掺杂导致电化学性能改善的原因不尽相同. 其中 $LiNi_{0.05}Co_{0.05}Mn_{1.9}O_4$ 样品因其较低的电化学极化和较大的 Li^+扩散系数而具有较好的电化学性能.

关键词: 锂离子电池, 掺杂锂锰氧尖晶石, 沉淀法, 电化学性质

中图分类号: O646

2005-04-05 收到初稿, 2005-05-09 收到修改稿.

联系人: 王建明 (E-mail: wjm@cmsce. zju. edu. cn; Tel: 0571- 87951513; Fax: 0571-87953309).

*国家自然科学基金(59902004)资助项目